ADVANCED MATERIALS
www.advmat.de

www.MaterialsViews.com

Color Depth Modulation and Resolution in Phase-Change Material Nanodisplays

*Carlos Ríos, Peiman Hosseini, Robert A. Taylor, and Harish Bhaskaran**

Color modulation has been a topic of longstanding interest in science and engineering given its multiple applications in display technology, smart glass, security marks, and active optical components.[1,2] Passive elements such as optical coatings employing a wide range of materials, multilayer configurations, or structured films have been extensively used in optical systems to obtain a full range of colors and spectral windows in both reflective and transmissive devices.[1–6] Moreover, active materials with unique physical or chemical properties such as electrochromism,[7–9] piezochromism,[10] plasmonic effect,[11] photoluminescence,[12,13] and volatile phase-change materials[14] have been exploited for color modulation purposes. The dynamic modulation of optical properties by such materials has given rise to remarkable resolution, low dimensionality, and low energy operation of displays.[15] However, a combination of both, i.e., a device with high-resolution featuring offline color retention while still allowing full-gamut modulation, had been elusive or had required external chemical agents[16] until recently, when an optoelectronic framework using nonvolatile nucleation dominated phase-change materials (PCMs) was proposed to fill this gap by employing $Ge_2Sb_2Te_5$ (GST) as the active bistable component.[17]

PCMs promise great potential given that state-of-the-art alloys are capable of switching in picoseconds timescales between two optically and electrically differentiable states in response to appropriate heat stimuli (crystallization) or melt-quenching processes (amorphization).[18–20] More interestingly, they present room temperature non-volatile behavior by stably retaining either state for years.[21–23] All these properties together mean that two highly differentiable optical states, allowed by the modulation in both the real and the imaginary refractive index under phase switching, are achievable within the same thin film; which in turn can be harnessed to switch colors.[17,24,25] The approach presented by Hosseini et al.[17] relies on the strong Fabry–Perot-type interference undertaken within a stack of layers featuring a highly absorptive medium,[6] GST in this case. By using such material, colors were obtained with just a few layers thus presenting low-dimensionality (70 to 300 nm for the whole stack), which in turns allows for flexible substrates to be employed. Furthermore, GST can be locally and reversibly switched at nanometric scales, enabling resolution beyond any other display previously reported. In this work, we demonstrate that $Ag_3In_4Sb_{76}Te_{17}$ (AIST), a growth dominated phase-change alloy,[26] can be employed for similar color modulation, but with better depth modulation capability (i.e., grayscale). We further demonstrate the limits of this technique in terms of resolution and switching energy. Lastly, we present a comparison between the performance of AIST and GST in terms of color modulation, resolution, and energy efficiency in devices constituted by uniform films.

We use optical cavities consisting of two transparent conducting layers of indium-tin oxide (ITO) sandwiching a thin film of PCM, either AIST or GST, on top of a mirror; as sketched in **Figure 1**a. ITO was selected among other optically transparent materials due to its remarkable electrical conductance,[27] which is useful for electrical switching as demonstrated later in this paper. In our devices, the top ITO layer has no effect on the color being reflected and it is used only to protect the PCM from oxidation; it is fixed to be 10 nm thick. On the other hand, the bottom ITO layer plays a crucial role as it is the medium inside the optical cavity between two ultra-thin absorptive layers. Therefore, the reflected color, i.e., the resonance condition of the cavity depends mainly on the thickness of this layer.

To engineer our devices such that the thickness of each layer is optimized for any specific color, we utilize the theory of thin-film optics to numerically calculate the total reflectance of an assembly of thin films using the algorithm detailed in ref. [1]. Using the continuity condition of the tangential electric (E) and magnetic (H) fields at each boundary and the directionality of the incident radiation, one can obtain the transmission through the bottom interface towards the substrate (given by the amplitudes E_{subs}, H_{subs}) and the total reflection towards air (from the incident amplitudes on the upper interface given by E_{air}, H_{air}) from the transfer matrix, i.e., the product of the matrices carrying the contribution of the local interference in each intermediate thin-film layer. This matrix is given by (for more details see ref. [1])

$$\begin{bmatrix} E_{air}/E_{subs} \\ H_{air}/E_{subs} \end{bmatrix} = \begin{bmatrix} B \\ C \end{bmatrix} = \left\{ \prod_{r=1}^{q} \begin{bmatrix} \cos\delta_r & i\sin\delta_r/\eta_r \\ i\eta_r \sin\delta_r & \cos\delta_r \end{bmatrix} \right\} \begin{bmatrix} 1 \\ \eta_m \end{bmatrix} \quad (1)$$

Where $\delta_r = \frac{2\pi d_r}{\lambda}\left(n_r^2 - k_r^2 - n_0^2 \sin^2\vartheta_0 - 2i\, n_r k_r\right)^{\frac{1}{2}}$ is the phase introduced to the incident light by the thickness d_r of the film

C. Ríos, Dr. P. Hosseini,[+] Prof. H. Bhaskaran
Department of Materials
University of Oxford
Parks Road, Oxford OX1 3PH, UK
E-mail: harish.bhaskaran@materials.ox.ac.uk
Prof. R. A. Taylor
Department of Physics
Clarendon Laboratory
Parks Road, Oxford OX1 3PU, UK
[+]Present address: Bodle Technologies Limited, Begboke Science Park, Begbroke, Oxford, OX5 1PF, UK

DOI: 10.1002/adma.201506238

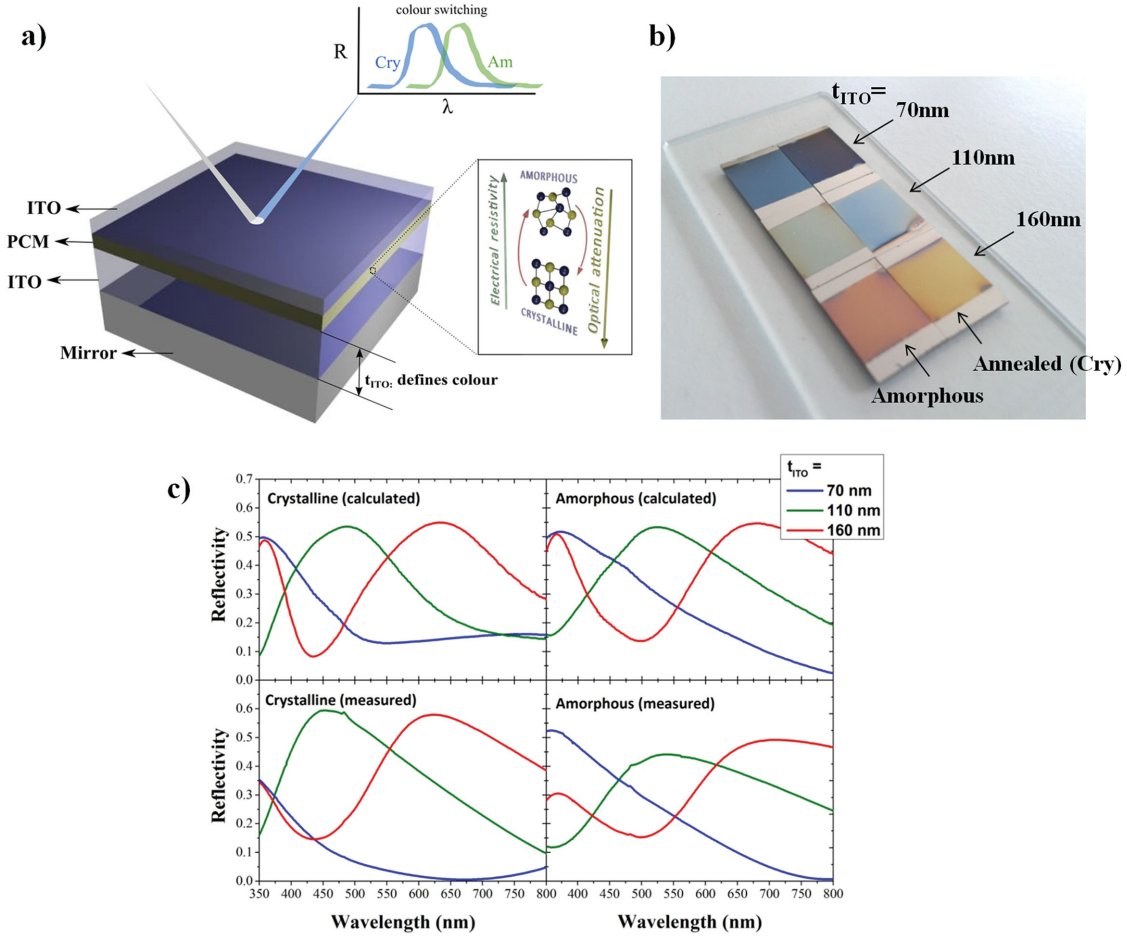

Figure 1. Color modulation using AIST thin films. a) Schematic diagram of the multilayer stack and the principle of operation. b) An image demonstrating color modulation obtained upon phase switching under natural sunlight on films stacks of 10 nm ITO/7 nm AIST/t_{ITO} ITO where t_{ITO} = 70 nm, 110 nm, and 160 nm are shown. c) Calculated and measured reflectance spectrum for the samples shown in b), where crystalline corresponds to the phase state reached after annealing.

r (r = 1 being the upper layer) with complex refractive index $N_r = n_r + ik_r$. The incident light strikes the first layer at an angle ϑ_0. η_r is the tilted optical admittance, either $\eta_r = \gamma n_r cos\vartheta_r$ for TE or $\eta_r = \gamma n_r / cos\vartheta_r$ for TM polarized incident light, with γ being the optical admittance defined as function of the electrical permittivity (ε_0) and the magnetic permeability (μ_0) as $\gamma = (\varepsilon_0/\mu_0)^{1/2}$. The sub index m is for the substrate medium and the subindex o stands for the incident medium. From the transfer matrix equations and by introducing the wavelength, incoming angle, refractive index, thickness of each layer and the incoming angle the total reflectance can be computed as[1]

$$R = \left| \frac{\eta_0 B - C}{\eta_0 B + C} \right|^2 \tag{2}$$

We used this algorithm to engineer the AIST-based samples shown in Figure 1b, presenting distinct colors as a function of ITO thickness and PCM crystallographic state. We found good agreement between the calculated and the measured spectra for different ITO thicknesses presented in Figure 1c, where a wavelength blue-shift up to 50 nm takes place upon material switching to crystalline state. Crystallization of as-deposited AIST was obtained after annealing for 5 min at 250 °C on a hotplate.

We then demonstrated the application of these devices in nanodisplays. Samples with PCMs in as-deposited amorphous state were switched locally by applying a voltage bias between a conductive atomic-force microscopy (AFM) cantilever and the ITO film under the PCM, as sketched in **Figure 2**a. Using the high electrical conductivity of ITO, nanopixels can be modified one at the time by Joule heating of the PCM, which switches it to crystalline state. This can be done locally either by switching points independently, or by modulating the applied voltage while scanning the surface. Using scanning mode and setting 0 V to black and 7 V to white, we were able to create 70 × 70 µm binary images onto the PCM layer as shown in Figure 2b. These images present an outstanding resolution with features as small as 500 nm. In this demonstration, we use an AFM to electrically write nanopixels, because of which the impedances are not perfectly matched. This means we are unable, under the current experimental conditions, to get nanosecond pulses required to erase, i.e., to reamorphize a nanopixel. However, we have previously reported in Hosseini et al.[17] that on-chip crossbar devices are able to readily write and erase pixels multiple

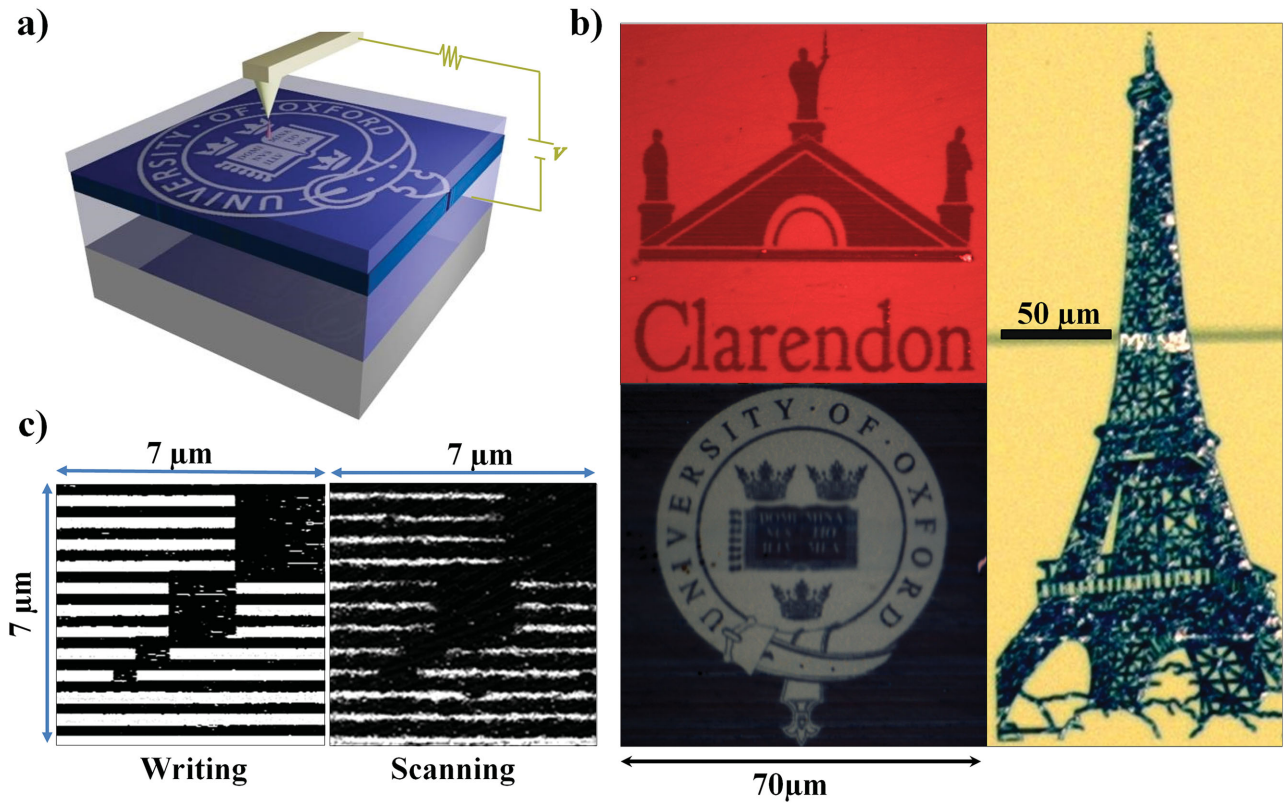

Figure 2. Nanodisplay applications of AIST. a) Sketch of the experimental setup. Conductive AFM is used to locally switch AIST by applying voltage between the two ITO layers. b) Optical microscope images of electrically written objects on continuous ITO/AIST/ITO/Pt stacks with different colors. c) Voltage modulation using CAFM of a 7 µm × 7 µm binary image – 0 V for black and 10 V for white areas (left); constructed image read electrically by scanning with a 0. 5 V bias (right).

times by switching electrically GST within multilayer configurations that allow for reflected colors. Thus, with erasability and re-writing capability already demonstrated, we focus on further capabilities, properties, and limits of the PCM nanodisplays instead.

In Figure 2c, a 7 µm × 7 µm image is transferred to AIST using electrical switching on the stack. The voltage had a few anomalous variations while modulating the signal due to the experimental challenges of scanning a small area, as seen in the Writing image; this corresponds to the image that the AFM wrote (i.e., modulated electrically). Given the resolution limit of optical microscopes, they are no longer capable of producing an accurate visualization of the image. Instead, we used the same AFM to inspect the image that has been transferred by creating an image from the changes in resistance of the surface. In this case, we applied 0.5 V, which is lower than the crystallization threshold but enough to differentiate the resistivity of the two states of the sandwiched PCM. This approach allows us to retrieve the image as shown in the scanning image in Figure 2c, where white areas represent more conductive, crystalline areas. Despite the modulation deficiencies and the randomness of the crystalline nuclei generation, the image reproduces the original one at this scale with features down to ≈250–300 nm.

The amount of crystallized PCM in a certain scanned area is linked to the final color perception of the image. If the separation between two nuclei is smaller than the size they grow after applying a voltage pulse then we would have a fully crystallized area in between, therefore the color will correspond completely to that of crystalline state. On the other hand, if the separation is larger, then some amorphous material will remain in between and therefore the color will adopt an intermediate state between that of the amorphous and crystalline. In our particular experiment, the size of the nuclei is determined by the voltage, while the separation is determined by the scanning speed. To corroborate this, we applied voltages of 2, 4, 6, 8 and 10 V while scanning at a fixed frequency of 1 Hz onto a 70 µm × 70 µm square sample with 10 nm ITO/7 nm AIST/70 nm ITO layers. The results are shown in **Figure 3**a, where the color clearly gets deeper, i.e., closer to that completely crystalline as the voltage increases. Moreover, we found that even 2 V is observed to be enough to induce color switching, although with lower contrast, given that the crystallization threshold was measured to be 1.40 ± 0.05 V as detailed below. Subsequently, we mapped the 0 to 255 gray level scale to a continuous 0 to 10 V for the electrical pulses applied during CAFM scanning. By doing so, we were able to write the $70 \times 70\ \mu m^2$ grayscale image shown in Figure 3b on a 10 nm ITO/7 nm AIST/70 nm ITO sample with perceptible color depth modulation, as depicted in the optical microscope image in Figure 3c. Lower voltages corresponding to those darker areas in the original image led to lower contrast in the written image as the color switching is not significantly high and the material remains mostly in amorphous state. However,

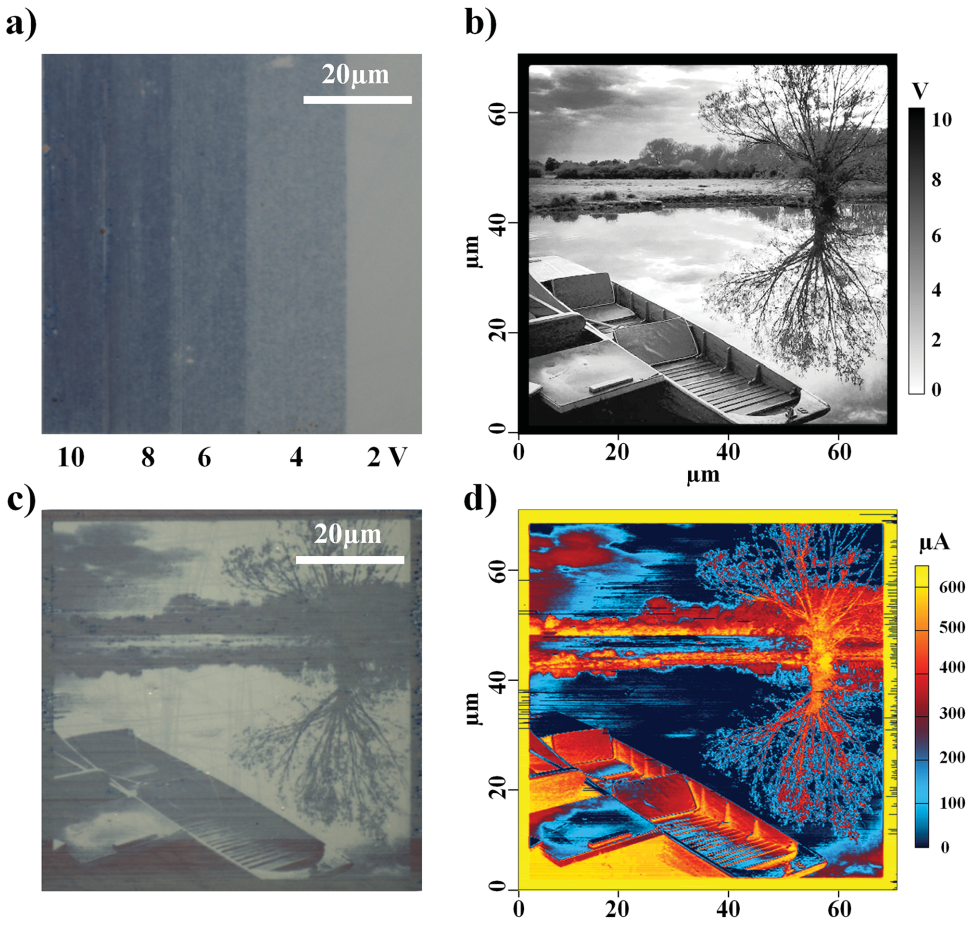

Figure 3. Grayscale images rendering. a) Scanning voltage varying between 0 and 10 V induce different levels of crystallization and therefore, different color in reflection mode. b) Image with the equivalent map between greyscale and voltage for the electrical pulses applied during the scanning. c) Optical microscope image of the picture in (b) written on 70 × 70 μm^2 of AIST. d) Conductivity measurement while the image (c) is written in scanning mode. a) and c) were written using CAFM on 10 nm ITO/7 nm AIST/ 70 nm ITO/Pt samples.

for voltages larger than 4 V, the color is clearly and continuously modulated to intermediate states between the amorphous and the crystalline phases allowing for a "grayscale" image.

For a better visualization of the crystallization that takes place during the scanning, we mapped the corresponding "electrical image" (caused by the change in electrical resistance) by measuring the current through the ITO/AIST/ITO stack while scanning in a CAFM. The results are shown Figure 3d, where the different degrees of crystallization are visible as variations in conductance when switching takes place. The conductivity changes due to partial crystallization (with voltages over the threshold) present better contrast than the reflectivity changes. Therefore, the "electrical image" is more detailed than its optical counterpart allowing for a better differentiation of intermediate states.

We use the transfer matrix in Equation (1) to study the differences and similarities in color generation and modulation between devices containing both GST and AIST. In order to have a more comprehensive understanding on how the colors on the devices are really perceived by the human eye, we calculated from the reflectance spectrum obtained in Equation (2), all the achievable colors using the XYZ tristimulus[28] values as a function of PCM and ITO thicknesses for both the amorphous and the crystalline phases. Subsequently, we plotted the XY color gamut on a chromaticity diagram as shown in **Figure 4**. Here, we varied the ITO thickness from 0 to 300 nm (one mark per 5 nm), which covers a vast range of colors in both phase states of the PCMs. From these results, we observe very similar color gamut in amorphous phase for both AIST and GST. The performance of both materials is quite similar due to the similarity of their complex refractive indices, which is dominated by the SbTe optical properties (see Figure S1, Supporting Information).[29,30] This can also be inferred by comparing the experimental spectra for AIST in Figure 1a with previously reported experiments for GST in ref. [17]. However, when both materials are switched to the crystalline state, AIST presents a similar but broader color gamut than GST only if the PCM layer is 6 nm or thicker. For thicknesses of 2 nm, the slight difference in the refractive index between the two materials plays a significant role in influencing the interference conditions; as it is seen for this case only, GST allows for a better color modulation. This could be a considerable advantage for GST,

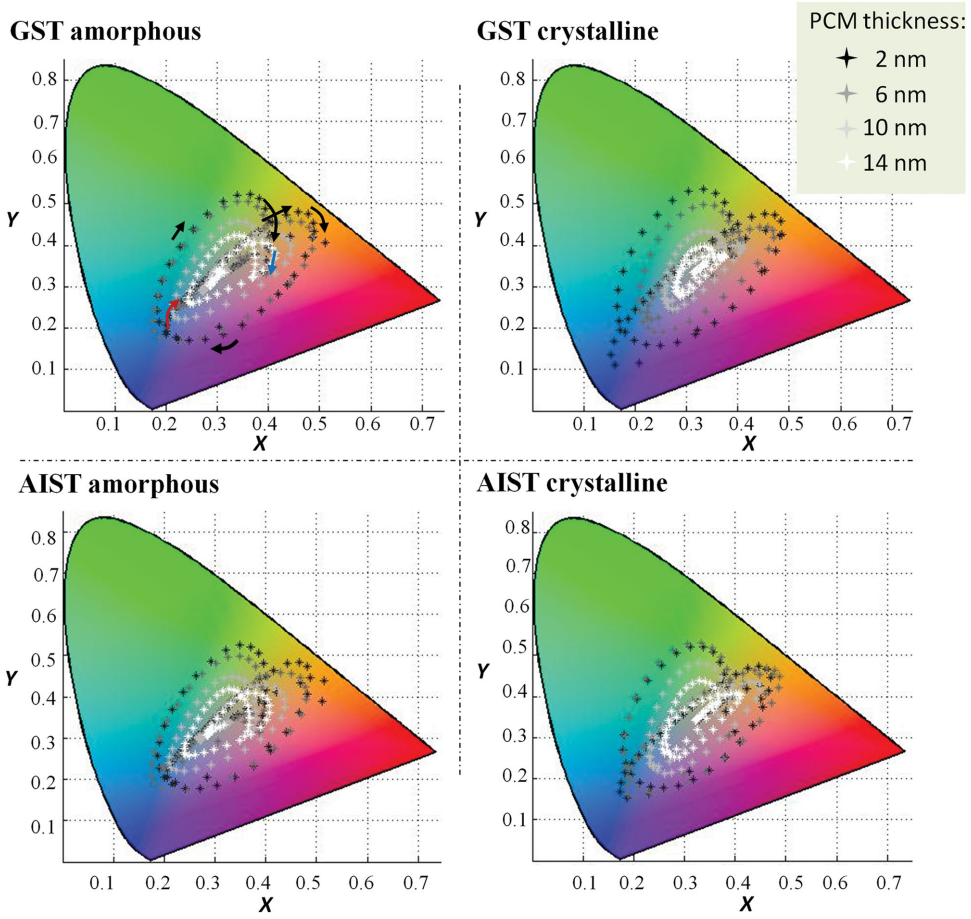

Figure 4. Color gamut comparison between AIST and GST. Calculated XY Color gamut on the chromaticity diagram for ITO/PCM/ITO/Pt samples. The bottom ITO spacer is swept from 0 to 300 nm in steps of 5 nm (one step = one mark on the graph) to study the resulting color when the PCM, either AIST or GST, present four different thicknesses. On the top left panel, the arrows start with the red one (0 nm ITO) and finish with the blue one (300 nm ITO) show the direction for increasing ITO thickness (for all figures and thicknesses).

as thinner films lead to greater color contrast upon switching. Furthermore, we calculated the wavelength at peak maximum spectra as a function three parameters—phase state, ITO and PCM thickness—as presented in Figure S2 (Supporting Information) for AIST and GST. Reflectance peaks centered in any color in the visible spectrum are achievable for both materials by changing only the ITO spacer dimensions. Moreover, the same device (i.e., same ITO spacer thickness) leads to similar color when using either phase-change alloy notwithstanding the different nature of their crystallization processes. The effect of the thickness of the PCMs only results in a slight red-shift in the spectrum as it gets thicker in both cases. However, the blue-shift resulting from the high-to-low real refractive index and low-to-high extinction coefficient change, when switching from amorphous to crystalline state, is definitely more pronounced and the reason why the color switching is possible. Considering the shift between spectra in amorphous and crystalline (for ITO thicknesses in the range 100–160 nm), AIST presents, on an average, a modest peak shift of 6 nm larger than for GST.

To study the resolution allowed by each material and the energy required to switch, we used conductive AFM to locally switch one pixel and compare the resulting nuclei sizes and IV curves. Although uniform layer samples were used in these experiments, structured samples featuring ITO/PCM/ITO stack nanopillars on top of the mirror were employed without considerable differences. Triangular-shaped pulses from 0 to 10 V were applied to randomized pixels to crystallize the PCM. Subsequently, we scan the surface while applying a constant voltage of 0.5 V in order to visualize changes in conductivity, and therefore the nuclei generated in the previous step. Electrically imaged nuclei are depicted in **Figure 5**a for AIST and Figure 5c for GST. A large voltage of 10 V was used for the sake of visualization given that lower voltages induced weak transitions that are not visible in an AFM. Together with changes in conductivity, we observed surface height variation ranging from 2 to 4 nm, as expected due to the volume expansion of PCMs under crystallization.[31] Direct comparison leads to the inference that AIST, because of its growth dominated nature, presents larger and denser nuclei. On the other hand, GST presents smaller and more dispersed nuclei characteristic of nucleation dominated materials. The corresponding *I–V* curves from the previous experiments are plotted in Figure 5b,d. There is good agreement between the current measured at 0.5 V when switching with a 0–10–0 V triangular pulse (*I–V* curve)

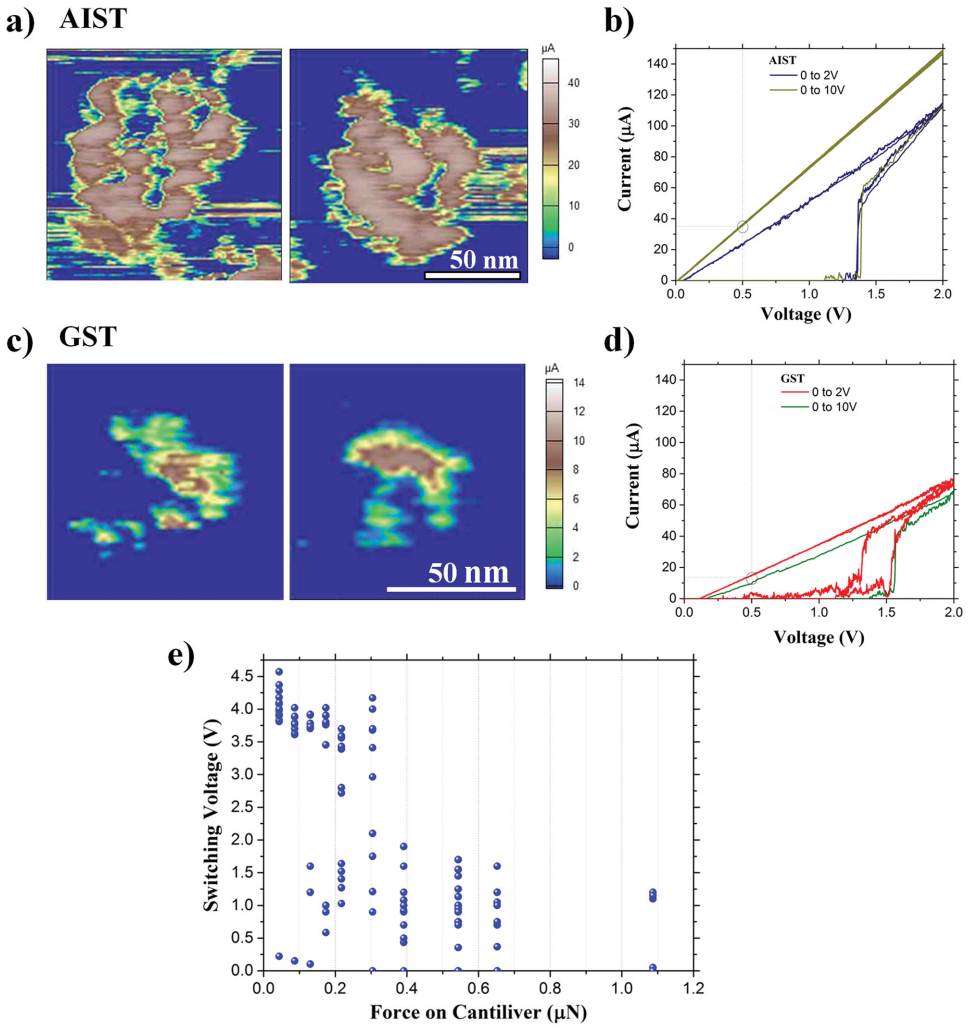

Figure 5. Resolution and electrical switching comparison between GST and AIST. a) Two AIST nuclei (nanopixel) generated with a 0 V–10 V–0 V triangular electrical pulse using CAFM and reconstructed by electrically scanning the area with a 0.5 V bias. b) Characteristic *I–V* curves during AIST switching. The 0 to 10 V ramp data (shortened for the sake of visualization) correspond to that in a). The highlighted region corresponds to the *I–V* characteristics at 0.5 V. The corresponding current is in good agreement with the value measured for the crystalline areas in a). 0 to 2 V ramps are also plotted to demonstrate the minimum bias voltage required to properly switch the material, although the size of the nuclei is much smaller, therefore difficult to visualize. c) and d) analogous to a) and b) but for GST. e) Switching voltage vs. force on cantilever (set point) when realizing 0 to 5 V *I–V* measurements. Dots at 0 V mean that there was a short circuit at that specific point.

and the current measurements when scanning the nuclei with 0.5 V in the scales of Figure 3c,e. *I–V* curves from 0 to 2 V are also plotted to measure the crystallization threshold, which for AIST is 1.40 ± 0.15 V and 1.50 ± 0.15 V for GST. It is important to take into account the resistance of the tip and ITO top layer and the possible impurities on the tip or on the surface and their effect on the measured *I–V* characteristics, especially the threshold voltage. Those impurities and other possible interface phenomena meant that switching voltages ranging from ≈1 to ≈5 V were obtained while writing, thus increasing the uncertainty of the measurement. Because of this, even though results for GST suggest a larger crystallization threshold, it is not considerably higher than for AIST; from a practical point of view, both devices behave identically.

However, to understand the nature of the huge variation of the switching voltage described above, we made measurements with 0 to 5 V triangular pulses in contact mode with the top of the uniform films but by varying the force applied to the AFM tip. Results in Figure 5e clearly demonstrate that the higher the force, the lower the switching voltage, as the tip makes better contact with the top ITO layer (top electrode) and overcomes any surface dirt. To obtain reliable and repeatable switching voltages, forces over a threshold of 400 nN are required.

In conclusion, we demonstrate that the growth dominated AIST can be used as an active material to obtain off-line color modulation with voltages as low as 2 V and resolutions down to 300 nm in scanning mode and less than 50 nm in pixel-by-pixel mode employing multilayer optical cavities. Furthermore, we presented the very first demonstration of non-binary color rendering on a single device (pixel) by exploiting the dependency of the degree crystallization on applied voltage. Using this, we achieved continuous "grayscale" images, which in turn adds a new degree

of functionality to the newly emerging field of PCM displays.[17,24] We then demonstrate that $Ge_2Sb_2Te_5$ and $Ag_3In_4Sb_{76}Te_{17}$ present very similar properties and performance. Finally, resolution limits below 50 nm are achievable in both materials, in the pixel by pixel approach, with differences in the nucleation formation due to the different crystallization dynamics of both materials. These results, together with previously reported capabilities such as reversible switching on cross-bar devices and the feasibility of nano-displays on flexible substrates, pave the way toward a new generation of bistable, ultra high-resolution and flexible display technologies in parallel with other potential applications in nanophotonics and optoelectronics.

Experimental Section

Sample Fabrication: Thermally grown SiO_2 wafers (IDB Technology, UK) were used as substrate for the devices. A standard cleaning process in acetone with ultrasonic agitation, isopropanol, distilled water, and dried nitrogen was used beforehand. All thin films were sputtered at room temperature using a Nordiko system in 100 sccm (standard cubic centimeters per minute) Argon atmospheres. Base pressures were around 3×10^{-7} Torr and a working pressure of 0.5 mTorr. The mirror was fabricated by depositing 100 nm of Platinum on top of the silica wafer. ITO (Testbourne, UK) was sputtered from a 3'' target at 120 W DC at a rate of 11 nm min^{-1}. $Ag_3In_4Sb_{76}Te_{17}$ and $Ge_2Sb_2Te_5$ (Super Conductor Materials, USA) were sputtered from 2.5'' solid targets at 30 W DC each at rates of and 3.4 and 3.6 nm min^{-1}, respectively.

Measurement Setup: The spectroscopic measurements were carried out in a Lambda 1050 spectrometer (Perkin Elmer, USA) in reflection mode. The measurements were calibrated against commercial aluminum standards within the wavelength range 350–750 nm. We used conductive AFM (Asylum Research MFP-3D) using ORCA accessories with conductive diamond tips (Bruker) to realize, in contact mode, the measurements of nuclei size in Figure 5a–d and Cr/Pt Multi75E-Gto measure the switching voltage versus force data in Figure 4e. Both tips were successfully tested to write binary and grayscale images.

Supporting Information

Supporting Information is available from the Wiley Online Library or from the author.

Acknowledgements

The authors acknowledge support by EPSRC grants EP/J018783/1, EP/J00541X/2 and EP/J018694/1 and the John Fell Fund. C.R. is grateful to JEOL UK and Clarendon Fund for funding his graduate studies.

Received: December 15, 2015
Revised: January 14, 2016
Published online: March 29, 2016

[1] H. A. Macleod, *Thin-Film Optical Filters*, CRC Press, Bristol, UK, **2010**.
[2] P. Yeh, *Optical Waves in Layered Media*, Wiley, New York **1988**.
[3] M. S. Ünlü, S. Strite, *J. Appl. Phys.* **1995**, *78*, 607.
[4] P. Yeh, A. Yariv, A. Y. Cho, *Appl. Phys. Lett.* **1978**, *32*, 104.
[5] M. A. Kats, F. Capasso, *Appl. Phys. Lett.* **2014**, *105*, 131108.
[6] M. A. Kats, R. Blanchard, P. Genevet, F. Capasso, *Nat. Mater.* **2013**, *12*, 20.
[7] C. Granqvist, *Solid State Ionics* **1992**, *53–56*, 479.
[8] P. Monk, R. Mortimer, D. Rosseinsky, *Electrochromism and Electrochromic Devices*, Cambridge University Press, Cambridge, UK, **2007**.
[9] R. H. Yan, R. J. Simes, L. A. Coldren, *IEEE Photonics Technol. Lett.* **1989**, *1*, 273.
[10] A. Seeboth, D. Loetzsch, R. Ruhmann, *Am. J. Mater. Sci.* **2012**, *1*, 139.
[11] S. J. Tan, L. Zhang, D. Zhu, X. M. Goh, Y. M. Wang, K. Kumar, C.-W. Qiu, J. K. W. Yang, *Nano Lett.* **2014**, *14*, 4023.
[12] T. S. Enda, Y. C. Ho, T. H. Irakawa, H. O. Kamoto, *Jpn. J. Appl. Phys.* **2000**, *39*, 4716.
[13] A. C. Arsenault, T. J. Clark, G. von Freymann, L. Cademartiri, R. Sapienza, J. Bertolotti, E. Vekris, S. Wong, V. Kitaev, I. Manners, R. Z. Wang, S. John, D. Wiersma, G. A. Ozin, *Nat. Mater.* **2006**, *5*, 179.
[14] M. A. Kats, D. Sharma, J. Lin, P. Genevet, R. Blanchard, Z. Yang, M. M. Qazilbash, D. N. Basov, S. Ramanathan, F. Capasso, *Appl. Phys. Lett.* **2012**, *101*, 221101.
[15] A. C. Arsenault, D. P. Puzzo, I. Manners, G. A. Ozin, *Nat. Photonics* **2007**, *1*, 468.
[16] H. Fudouzi, Y. Xia, *Langmuir* **2003**, *19*, 9653.
[17] P. Hosseini, C. D. Wright, H. Bhaskaran, *Nature* **2014**, *511*, 206.
[18] C. Ríos, M. Stegmaier, P. Hosseini, D. Wang, T. Scherer, C. D. Wright, H. Bhaskaran, W. H. P. Pernice, *Nat. Photonics* **2015**, *9*, 725.
[19] J. Siegel, A. Schropp, J. Solis, C. N. Afonso, M. Wuttig, *Appl. Phys. Lett.* **2004**, *84*, 2250.
[20] S. Raoux, F. Xiong, M. Wuttig, E. Pop, *MRS Bull.* **2014**, *39*, 703.
[21] D. Lencer, M. Salinga, B. Grabowski, T. Hickel, J. Neugebauer, M. Wuttig, *Nat. Mater.* **2008**, *7*, 972.
[22] S. R. Ovshinsky, *Phys. Rev. Lett.* **1968**, *21*, 1450.
[23] S.-H. Lee, Y. Jung, R. Agarwal, *Nat. Nanotechnol.* **2007**, *2*, 626.
[24] P. Hosseini, H. Bhaskaran, *Proc. SPIE* **2015**, *9520*, 95200M.
[25] F. F. Schlich, P. Zalden, A. M. Lindenberg, R. Spolenak, *ACS Photonics* **2015**, *2*, 178.
[26] B.-S. Lee, R. M. Shelby, S. Raoux, C. T. Retter, G. W. Burr, S. N. Bogle, K. Darmawikarta, S. G. Bishop, J. R. Abelson, *J. Appl. Phys.* **2014**, *115*, 063506.
[27] H. Kim, C. M. Gilmore, A. Piqué, J. S. Horwitz, H. Mattoussi, H. Murata, Z. H. Kafafi, D. B. Chrisey, *J. Appl. Phys.* **1999**, *86*, 6451.
[28] H. Levkowitz, *Color Theory and Modeling for Computer Graphics, Visualization, and Multimedia Applications*, Springer Science & Business Media, Norwell, MA, USA, **1997**.
[29] S. Y. Kim, S. J. Kim, H. Seo, M. R. Kim, *Proc. SPIE* **1998**, *3401*, 112.
[30] Z. Guang-Jun, G. Dong-Hong, G. Fu-Xi, *Chin. Phys.* **2005**, *14*, 0218.
[31] K. Do, D. Lee, D.-H. Ko, H. Sohn, M.-H. Cho, *Electrochem. Solid-State Lett.* **2010**, *13*, H284.